LASER & PHOTONICS REVIEWS

www.lpr-journal.org

Controllable Dynamic Single- and Dual-Channel Graphene Q-Switching in a Beam-Splitter-Type Channel Waveguide Laser

*Ji Eun Bae, Thomas Calmano, Christian Kränkel, and Fabian Rotermund**

Direct inscription of structures by femtosecond-laser pulses facilitates the flexible fabrication of diverse optical channel waveguides in dielectric laser gain media. Among them, beam-splitter-type waveguide lasers have been recently studied; however, there is a lack of investigations on the effect of unique characteristics of such waveguides, such as controlled splitting ratios of output powers and selectable excitation of individual channels, for pulsed laser operation. Here, dynamic single- and dual-channel graphene Q-switching of an Yb:YAG waveguide consisting of one input and two output channels is demonstrated by controlling the power-splitting ratio. Single-channel Q-switched operation, exhibiting typical Q-switched pulses, is achieved by interaction between the graphene saturable absorber and the desired one of the two channels. When both channels exceed the Q-switching threshold, dual-channel Q-switching generates a pulse train that simultaneously combines the separately Q-switched pulses induced from each channel under excitation with a single pump source. At a fixed power-splitting ratio, the pulsed mode can be dynamically switched between the single- and dual-channel Q-switched operations by varying the pump power. The beam-splitter-type waveguide laser demonstrated in this study can be further developed for multiple-channel Q-switching, high-repetition-rate mode-locking, and on-chip dual-comb sources advantageous for diverse applications in optical communication, metrology, and sensing.

1. Introduction

Optical waveguides (WGs) are essential components of integrated photonics. This approach is applicable to active amplifiers, laser oscillators, as well as passive functional devices, such as couplers and modulators. In particular, the inscription of WG structures inside laser gain media by intense laser pulses is a prevalent strategy for downsizing solid-state lasers to an on-chip handheld scale, owing to effectively confined light propagation within micrometric or even submicrometric volumes. To fabricate channel WGs in dielectric crystalline materials, the femtosecond direct laser writing (fs-DLW) technique has been increasingly utilized to facilitate complex 3D geometries and permanent refractive index changes in the volume of crystals without any plastic deformation.[1,2] In addition to straight channels, on-demand curve-shaped channel WGs based on fs-DLW have been demonstrated and provide significant potential for diverse functional optical elements.[3,4]

Beam-splitter-type (BS) WGs fabricated by fs-DLW are used not only in passive devices,[5,6] but also for continuous-wave (cw) laser operation in the 1[7–9] and 2 μm[10] wavelength range. Such BS WG lasers providing multiple lasing output signals from a single pump could be utilized in quantum optics, optical sensing, and communication applications. So far, pulsed operation of a BS WG laser has only been demonstrated in a passively Q-switched Nd^{3+}-doped $Y_3Al_5O_{12}$ (Nd:YAG) BS WG.[11,12] The lasers were pumped by a Ti:sapphire laser and the Nd:YAG BS WGs were based on the depressed-cladding WG structure consisting of 10 or more arrayed tracks. In these investigations, the Q-switched operation was demonstrated for a particular power splitting ratio close to 50:50 by using few-layer graphene and the separation of two outputs were less than 100 μm. In the present study, we focus, for the first time, on an Yb^{3+}-doped YAG (Yb:YAG) double-track BS WG laser that permits efficient Q-switched operation and actively tunable power splitting ratios with diode-pumping. In our previous report on the cw operation of the Yb:YAG BS WG,[7] the high output powers and slope efficiencies with variable splitting ratios were characterized in a compact cavity configuration without laser mirrors, which

J. E. Bae, F. Rotermund
Department of Physics
Korea Advanced Institute of Science and Technology (KAIST)
Daejeon 34141, Korea
E-mail: rotermund@kaist.ac.kr
T. Calmano
Institute für Laser-Physik
Universität Hamburg
Hamburg 22761, Germany
C. Kränkel
Zentrum für Lasermaterialien
Leibniz-Institut für Kristallzüchtung (IKZ)
Berlin 12489, Germany

The ORCID identification number(s) for the author(s) of this article can be found under https://doi.org/10.1002/lpor.202100501

DOI: 10.1002/lpor.202100501

is beneficial for device integration. The output channel separations between 81 and 647 μm were used with different radii of curvature of the splitting WG part. In terms of developing high-power miniaturized laser systems in the 1 μm wavelength range, diode-pumped Yb:YAG lasers are also beneficial due to their low quantum defect (Stokes shift) between the pump and laser wavelength and a subsequent low heat generation.[2,13–16]

One of the most critical conditions for a suitable saturable absorber (SA) for passive Q-switching or mode-locking of compact lasers is its flexible integrability in a laser cavity. Low-dimensional nanocarbons such as graphene and carbon nanotubes have been successfully recognized as suitable SAs in Q-switched[17–21] and mode-locked Yb^{3+}-doped fs-DLW WG lasers.[22–25] They exhibit superior optical properties including ultra-broadband nonlinear absorption, large nonlinearity and ultrafast relaxation time, and enable a relatively low cost and facile fabrication process.[26,27] In addition, they possess a high level of robustness and chemical (environmental) stability compared with other nanomaterials.

In this study, we present a novel dual-channel Q-switched operation using a fs-DLW BS Yb:YAG WG laser with one input and two output channels, utilizing monolayer graphene as the SA. By integrating graphene SAs on two output channels of the BS WG, stable passive Q-switching is achieved, and the Q-switched pulse trains from both output channels show identical pulse repetition rate and pulse duration. The output laser power splitting ratios can be varied depending on the incoupling position of the pump beam. A dynamic change in the pulsed sequence is observed between single- (Channel 1 or Channel 2) and dual-channel Q-switching by modifying the pump power splitting ratio and thus the laser power interacting with the graphene SA. Single-channel Q-switching is characterized by a conventional regular Q-switched pulse train. In the dual-channel Q-switching mode, a hybrid pulse train is observed, which combines the Q-switched pulses generated by each channel, resulting in two different pulse characteristics obtained with only one single pump source. The laser cavity consists of a graphene-integrated fs-DLW BS Yb:YAG WG and a pump mirror highly-reflective (HR) for the laser wavelength, ensuring simplicity and compactness with an output coupling ratio of 91%. The pulsed operation can be dynamically switched between single- and dual-channel Q-switching by adjusting the lateral position of the BS WG with respect to the pump. The overall pulse characteristics are analyzed in detail with respect to pump incoupling position and pump power. The present study is mainly focused on the validation of the striking dual-channel Q-switched operation and its controllability by a single pump source. Even though BS WG lasers have recently been recognized as an interesting approach with a strong potential,[7–12] the beam-splitting ratio as the parameter of paramount importance for BSs has previously been studied only for a particular splitting value and a widely tunable beam-splitting ratio in BS WG lasers has not been demonstrated so far.

2. Experimental Section

2.1. Fabrication of BS Yb:YAG Waveguide

The BS WG was inscribed by fs-DLW into a 9 mm long 7 at% Yb^{3+}-doped YAG crystal made from a Czochralski-grown boule provided by FEE GmbH. The 150 fs pulses from a 1 kHz Ti:sapphire chirped pulse amplifier (CPA-2010, Clark-MXR, Inc.) centered at a wavelength of 775 nm were focused ≈300 μm below the polished surface of the sample using a microscope objective with an NA of 0.65. The sample was moved by a high precision translation system (ABL1000, Aerotech Inc.). The three linear sections of the Y-shaped one-to-two BS WG were inscribed with a translation velocity of 25 μm s^{-1} superimposed by a 70 Hz sine oscillation with an amplitude of 2 μm to increase the index contrast.[3] In the curved sections, this sine oscillation was replaced by a zigzag-movement with an amplitude of 3.5 μm for technical reasons. Waveguiding based on Type-2 index modification[1] was achieved by inscribing parallel double tracks separated by 25 μm yielding guided beam diameters typically below 20 μm. Further details on the inscription process for curved WGs are found in the previous reports.[3,7] The two mirrored s-shaped sections forming the BS WG utilized in this study were each composed by two counter-bent circular arcs with a radius of curvature of 40 mm covering an arc angle of ≈2.6°. The resulting separation of the parallel sections of the two output channels amounts to 162 μm. Optical microscope images of the input facet and the splitting section of the BS WG are shown in **Figure 1**.

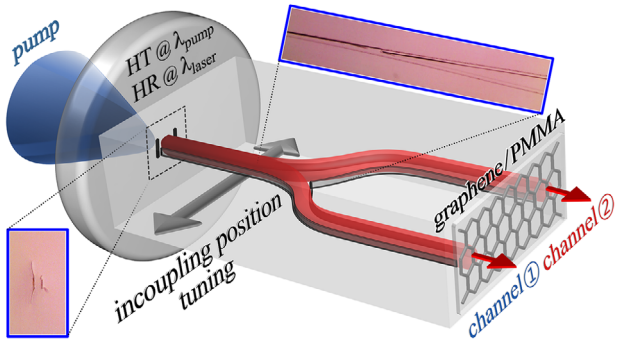

Figure 1. Experimental setup for dynamic Q-switching of Yb:YAG channel BS WG laser. Optical microscope images (blue boxes) represent the input channel and splitting section of the fs-DLW BS Yb:YAG WG.

2.2. Fabrication of Monolayer Graphene Saturable Absorber

Monolayer graphene grown via chemical vapor deposition on copper foil was used as the SA for passive Q-switching of the BS Yb:YAG WG. For the supporting and buffer layers of the graphene SA, polymethyl methacrylate (PMMA) was dissolved in chlorobenzene at a concentration of 50 mg mL^{-1}. The PMMA solution was spin-coated on the graphene with a thickness of ≈300 nm. The PMMA buffer layer can provide a sufficiently high mode field at the graphene SA by feedback from the Fresnel reflection at the interface between the PMMA layer and air. Subsequently, the copper foil was wet-etched, and the graphene/PMMA composite layer was rinsed in a distilled water bath. The graphene/PMMA was then transferred onto the polished output facet of the BS WG (Figure 1). Finally, the WG was baked in a vacuum oven. The image of the BS Yb:YAG WG covered by graphene/PMMA and the Raman spectrum of the pristine

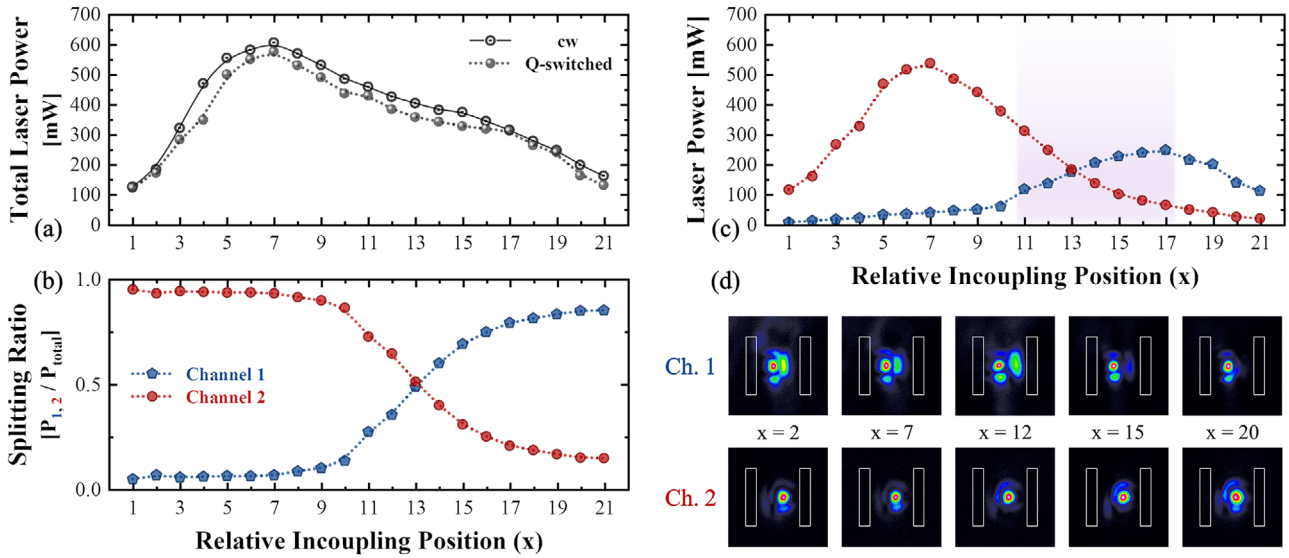

Figure 2. Laser performance characteristics measured versus the pump incoupling position (represented as x): a) Total laser output powers from both channels for cw and graphene Q-switched operation at the maximum incident pump power of 1.94 W (absorbed pump power depending on the position is given in Supporting Information S2). b) Output power splitting ratios and c) corresponding Q-switched output powers from each channel. d) Mode profiles of the laser beam from BS WG at the operation wavelength of 1030 nm for five different incoupling positions. The track cross-sections are indicated by white rectangles and the separation of the centers of the white bars is 25 µm.

monolayer graphene are shown in the Supporting Information S1. Details on the fabrication process of the graphene SA and its transfer applicable for WG lasers can be found in the previous work.[18]

2.3. Experimental Setup for Dynamic Q-Switching Experiments

The schematic of the laser setup for the demonstration of the Q-switched operation is shown in Figure 1. A single-mode tapered amplified diode laser (TA Pro, Toptica Photonics, Inc.) emitting at 969 nm was used as the pumping source. The linearly p-polarized pump beam is focused onto the WG input facet with a diameter of 22 µm using an aspheric lens with $f = 11$ mm. Another aspheric lens with $f = 6.24$ mm is used after the output facet of the BS WG to collimate output beams from the both channels. The BS Yb:YAG WG with a graphene/PMMA composite SA layer was mounted on a multiaxis stage without any cooling element. To change the pump incoupling conditions, the sample was translated perpendicular to the pump beam and the performance was investigated at 21 different incoupling positions. Relative incoupling position (represented as x) coordinates were determined by the µm-screw rotation of the used translation stage. Consequently, the separation between $x = 1$ and $x = 21$ corresponds to about 20 µm. A plane dielectric mirror highly transparent (HT) at the pump wavelength and HR at the laser wavelength is directly attached parallel to the WG input facet. The Fresnel reflection from the WG output facet ($R \approx 9\%$) enables laser operation with sufficient feedback in the WG owing to the high optical gain of the Yb:YAG, providing a 91% output coupling ratio and compact cavity configuration for the WG laser. The total length of the cavity composed of graphene-integrated BS Yb:YAG WG and an HR mirror is ≈9 mm, determined by the WG length.

3. Results and Discussion

3.1. Tunable Beam-Splitting Performances

By moving the BS WG input facet perpendicular through the input pump beam, the laser output power splitting ratio was adjusted in cw as well as in Q-switched operation mode. The total laser output power depending on the pump incoupling position (represented as x in **Figure 2**a) was measured at the maximum incident pump power. The focused pump beam diameter at the input facet of the WG was 22 µm, and the separation between the WG tracks was 25 µm. Note that the absorbed pump power of the BS WG decreases at both ends of the incoupling position because of the imperfect lateral coupling to the WG and partial cutting of the pump beam. The incoupling-position-dependent absorbed pump power and pump splitting ratio were estimated from the measured residual pump power for each position (see the Supporting Information S2). The maximum total output powers from both arms of 606 and 576 mW were achieved at $x = 7$ (total absorbed pump power of 1.57 W) for cw and Q-switched operation, respectively. The output power in the Q-switched regime drops only slightly compared with the cw operation because of the low insertion losses of the graphene SA in the cavity with a high output coupling ratio of 91%. The laser emission for all operation modes was centered at ≈1030 nm with linear p-polarization.

The measured output power splitting ratios for each channel, depending on the pump incoupling position, are depicted in Figure 2b. The splitting ratio between the channels (Channel 1:Channel 2) can be adjusted from 5:95 to 85:15 through 50:50 by simply changing the incoupling position into the WG, leading to a redistribution of the pump power. Figure 2c shows the Q-switched output power from each channel obtained by

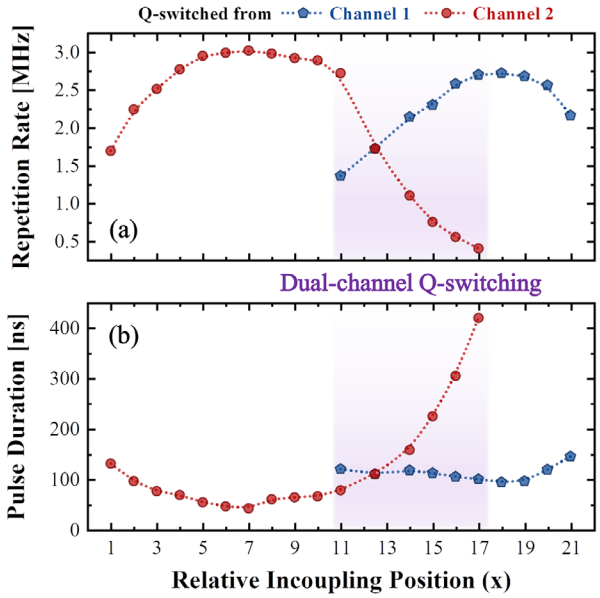

Figure 3. Q-switched pulse performance measured on the basis of the incoupling position. Dual-channel Q-switching is achieved at $x = 11$–17 and the other positions are single-channel Q-switched by Channel 1 ($x = 18$–21) or Channel 2 ($x = 1$–10): a) Pulse repetition rates and b) pulse duration (full-width at half-maximum).

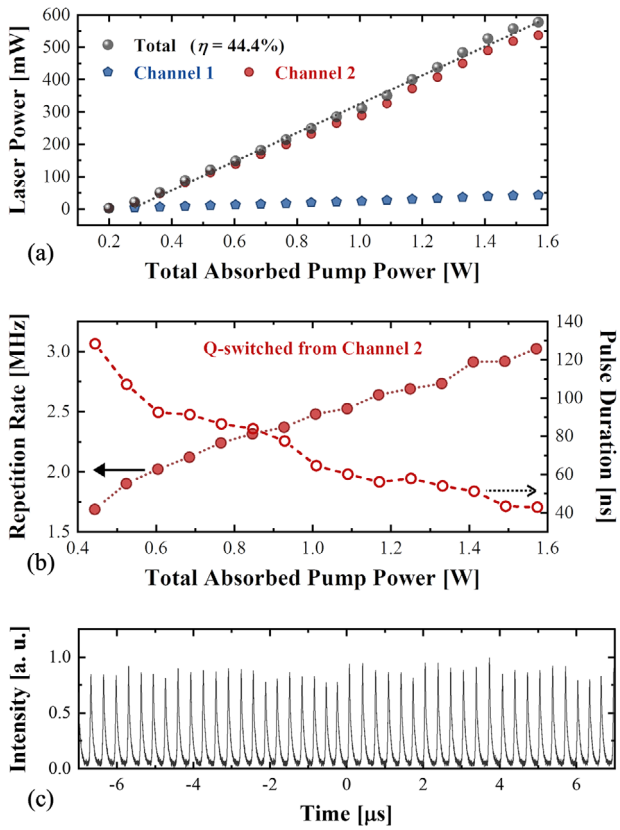

Figure 4. Single-channel (Channel-2) Q-switched laser performance characteristics measured at the incoupling position of $x = 7$: a) Laser output powers and b) pulse characteristics depending on the absorbed pump power. c) Sequence of Q-switched pulses at the absorbed pump power of 1.57 W. It should be noted that in the single-channel Q-switched regime the output from both arms exhibits identical repetition rate and pulse duration.

multiplying total output power (Figure 2a) and splitting ratio (Figure 2b). The laser beam profiles were measured from both output channels at various incoupling positions, as shown in Figure 2d. The intensity of the mode profile was normalized for each measurement.

3.2. Dynamic Single-Channel and Dual-Channel Q-Switching

Figure 3 shows the Q-switched pulse repetition rate and the pulse duration of the Q-switched BS WG laser for different incoupling positions at the maximum incident pump power. A dynamically Q-switched operation mode is achieved by controlling the pump incoupling position. Single-channel graphene Q-switching by Channel 1 or Channel 2 occurs at $x = 18$–21 and $x = 1$–10, respectively, representing a typical passively Q-switched WG laser operation. In this regime, the pulses emitted from both arms exhibit identical repetition rate and pulse length, albeit different pulse energy and thus average power. This is a clear indication for a pulse formation mechanism based on only one of the graphene SAs. For the intermediate incoupling positions of $x = 11$–17, dual-channel Q-switched pulses are generated by the interaction with the graphene SA deposited on both output channels. The coexistence of the doubly Q-switched pulse trains is the result of the mixed pulse oscillations in the BS WG cavity originating from both channels. The laser output from the dual-channel Q-switched BS WG emits a sequence of pulses with two different Q-switching frequencies. These observations indicate that the WG laser can dynamically generate single- and dual-channel Q-switched pulses through a simple change of the incoupling conditions by moving the BS WG.

The single-channel Q-switched operation indicates single pulse characteristics corresponding to pulses generated by each individual channel, while the dual-channel Q-switched regime shows the combination of two different types of pulse characteristics induced by both channels. Near the incoupling position of $x = 12$–13, an interesting degeneracy point is observed where the emitted pulse train exhibits single Q-switching characteristics with a repetition rate of 1.72 MHz and a pulse duration of 110 ns. This is exactly the case, where two pulsed modes operate under identical conditions in the dual-channel Q-switched regime. Note that the pulsed operation around this degeneracy point inevitably instable and thus difficult to characterize accurately. The characteristics of the pulses versus the incoupling position follow the trend expected from the laser output powers shown in Figure 2c. With higher output power, the repetition rate increases and the pulse duration decreases. It is important to note that the Q-switched pulses emitted from both channels of the BS WG exhibit identical pulse characteristics (see the Supporting Information S4).

In the case of the single-channel Q-switched operation mode, the shortest pulses with the highest average output power are achieved from the BS Yb:YAG WG laser at the position $x = 7$ from Channel 2. The laser power and pulsing performance were determined versus the absorbed pump power, as shown in **Figure 4**a,b,

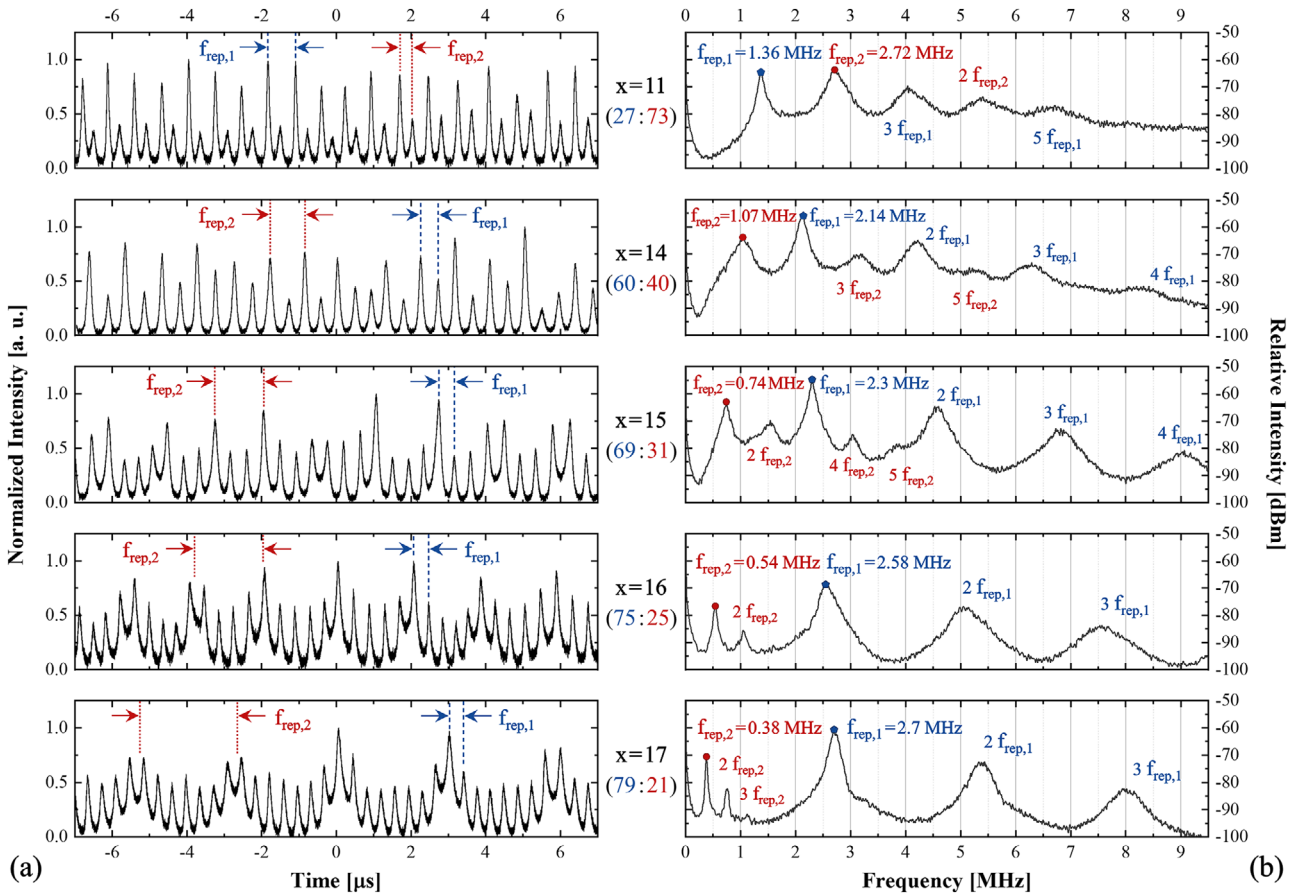

Figure 5. Dual-channel Q-switched laser pulse characteristics for the position of $x = 11$–17: a) Pulse trains and b) radio-frequency spectra. The fundamental frequencies Q-switched by Channel 1 and Channel 2 are denoted by $f_{rep,1}$ and $f_{rep,2}$, respectively.

respectively. In this position, the pulse trains Q-switched by the SA of Channel 2 were obtained at the outputs of both channels with an average output power splitting ratio between the channels of about 7:93. The total power slope efficiency was measured to be 44.4%, representing the highest efficiency ever achieved in a Q-switched BS WG laser. The single-channel Q-switched laser operates at a repetition rate of 3.02 MHz with a pulse duration of 42 ns at the maximum absorbed pump power of 1.57 W. The corresponding pulse energy amounts to 178 nJ from Channel 2 and 13 nJ from Channel 1, respectively (see the Supporting Information S5). The repetition rate increases from 1.68 MHz at 0.44 W absorbed pump power to 3.02 MHz at 1.57 W absorbed pump power, while the pulse duration decreases from 128 to 42 ns, respectively, indicating the typical fast-SA Q-switched pulse operation.[11,12] Below the Q-switching threshold absorbed pump power of 0.44 W, the laser operates in cw mode. The pulse train measured by an oscilloscope (1 GHz Tektronix, TDS7104) using a fast InGaAs photodiode revealed stable Q-switched operation (Figure 4c). For the other single-channel Q-switching positions, we found a similar behavior.

As indicated in Figure 3, the dual-channel Q-switched regime ($x = 11$–17) provides two separately generated Q-switched pulse characteristics. The dual-channel Q-switched pulse trains for different incoupling positions and consequently different power ratios are shown in **Figure 5**. The two dominant fast and slow frequency components for each pulse train can be appropriately distinguished. This was verified using a radio-frequency signal analyzer (Agilent N9020A). The fundamental peaks of two repetition rates ($f_{rep,1}$ and $f_{rep,2}$ induced by Channel 1 and Channel 2, respectively) are clearly identified and the corresponding harmonic frequencies were also measured. This confirms that the two Q-switched signals coexist in the dual-channel Q-switched regime. Based on the laser power tendency (Figure 2c), it can be concluded that the fast Q-switched frequency is generated by Channel 2, and the slower Q-switched frequency corresponds to Channel 1 at $x = 11$, while the situation is reversed for the incoupling positions $x = 14$–17. The results are consistent with the theoretical modeling of a fast-SA Q-switched laser (see the Supporting Information S3).

At the position $x = 11$, one of the dual-channel Q-switched positions, the pump-power-dependent laser powers were measured, as shown in **Figure 6**a, and a total power slope efficiency of 35.6% and an output power splitting ratio of 27:73 were obtained. Figure 6b demonstrates the corresponding Q-switched pulse parameters. At a maximum absorbed pump power of 1.65 W, Q-switched pulse repetition rates of 2.72 and 1.36 MHz with pulse durations of 72 and 120 ns are generated by Channel 2 and Channel 1, respectively. The corresponding pulse energy

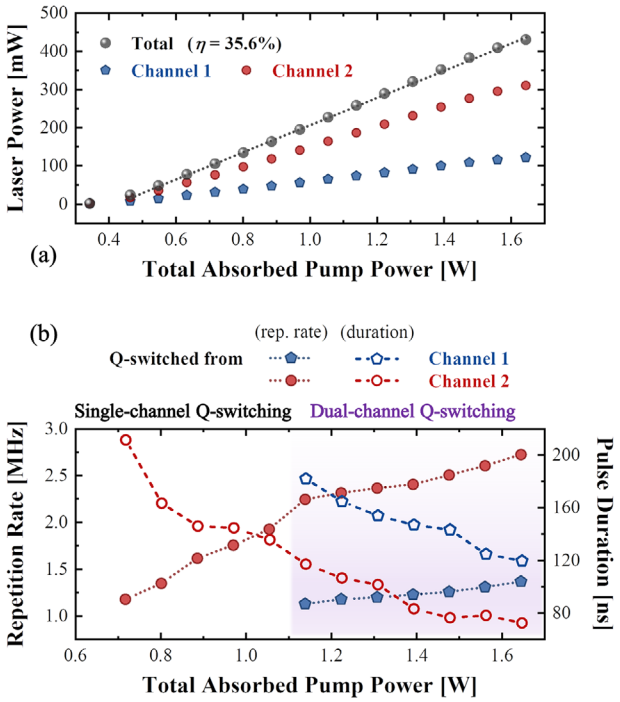

Figure 6. Q-switching characteristics measured at the incoupling position of $x = 11$: a) Laser output powers and b) pulse characteristics depending on the absorbed pump power. Dual-channel Q-switched operation at the maximum pump power is maintained up to the absorbed pump power of 1.14 W.

amounts to about 115 nJ from Channel 2 and 43 nJ from Channel 1, respectively. Note that the energy level of dual-channel Q-switched pulses can be evaluated by assuming the pulses in a typical pulse train, although an exact estimation of the pulse energy in the case of dual-channel Q-switching is difficult (see more in detail in S5 of the Supporting Information). By reducing the pump power, each pulse characteristic follows the expected Q-switching tendency of lower repetition rates and longer pulse durations. Below an absorbed pump power of 1.14 W, the output pulse train switches to a single-channel Q-switched operation. In the pump power range between 0.72 and 1.14 W, single-channel Q-switching is expected to be obtained by Channel 2. This is because Channel 1 delivers lower output power and inferior pulse performance. Consequently, its Q-switching threshold pump power is expected to be higher than for Channel 2, where it amounts to 0.72 W. These observations indicate that besides the pump incoupling position, the pump power is another degree of freedom to dynamically switch between single- and dual-channel Q-switching, even with different pulse characteristics for each operation mode. The variety of demonstrated passively Q-switched pulse trains and their controllability based on a widely tunable beam-splitting ratio is a novel Q-switching phenomenon observed in a 9-mm-long graphene embedded BS Yb:YAG WG laser with single pumping scheme.

4. Conclusion

Dynamic single- and dual-channel graphene Q-switching in an Yb:YAG fs-DLW BS WG laser was demonstrated by tuning the position of the pump beam with respect to the input channel of the BS WG and by changing the pump power level. Controlling the laser output power splitting ratio between Channel 1 and Channel 2 from 5:95 to 85:15 facilitates controlling the interacting power with the graphene SA, enabling the selective formation of Q-switched pulses by a specific channel. Consequently, it provides an efficient manner to dynamically switch the pulsed operation between single- and dual-channel Q-switching. Graphene is a suitable and robust material to be integrated as a SA into a compact monolithic WG cavity without an output coupler and to achieve both Q-switched operation modes demonstrated in this study. The single-channel Q-switching with the highest output power generates pulses with a repetition rate of 3.02 MHz and a pulse duration of 42 ns. In dual-channel Q-switching, the combination of two different types of pulse trains reveals the pulse-formation characteristics initiated separately from both channels only by single pump source. In addition, by changing the pump power, the Q-switching performance was analyzed in both pulsed regimes.

The obtained results suggest that the BS WG lasers can be further developed to realize GHz-repetition-rate mode-locking and on-chip dual-comb sources. The dual-channel Q-switched BS WG laser with potential power scaling[28] is advantageous to optical communication systems owing to its multiple modes that increase the capacity to meet the enhanced demands of data processing.[29,30] The BS Yb:YAG WG with an output channel separation of 162 μm also makes these devices suitable for efficient connection to optical fibers. The fs-DLW BS WG platform may also have potential applications in multiple-channel pulsed lasers with only a single-pumping source.

Supporting Information

Supporting Information is available from the Wiley Online Library or from the author.

Acknowledgements

This work was supported by the National Research Foundation (NRF) of Korea funded by the Korean Government (Nos. 2020R1A4A2002828 and 2019R1A2C3003504). J.E.B. acknowledges the NRF Global Ph.D. Fellowship (No. 2018H1A2A1061480).

Conflict of Interest

The authors declare no conflict of interest.

Data Availability Statement

The data that support the findings of this study are available from the corresponding author upon reasonable request.

Keywords

beam splitters, channel waveguides, femtosecond direct laser writing, graphene, passive Q-switching, waveguide lasers

Received: September 6, 2021
Revised: November 30, 2021
Published online:

[1] F. Chen, J. R. V. de Aldana, *Laser Photonics Rev.* **2014**, *8*, 251.
[2] T. Calmano, S. Müller, *IEEE J. Sel. Top. Quantum Electron.* **2015**, *21*, 401.
[3] T. Calmano, A.-G. Paschke, S. Müller, C. Kränkel, G. Huber, *Opt. Express* **2013**, *21*, 25501.
[4] L. Li, Z. Li, W. Nie, C. Romero, J. R. V. de Aldana, F. Chen, *J. Lightwave Technol.* **2020**, *38*, 6845.
[5] S. Nolte, M. Will, J. Burghoff, A. Tuennermann, *Appl. Phys. A* **2003**, *77*, 109.
[6] R. R. Thomson, T. A. Birks, S. G. Leon-Saval, A. K. Kar, J. Bland-Hawthorn, *Opt. Express* **2011**, *19*, 5698.
[7] T. Calmano, C. Kränkel, G. Huber, *Opt. Lett.* **2015**, *40*, 1753.
[8] Y. Jia, C. Cheng, J. R. V. de Aldana, F. Chen, *J. Lightwave Technol.* **2016**, *34*, 1328.
[9] H. Liu, J. R. V. de Aldana, M. Hong, F. Chen, *IEEE J. Sel. Top. Quantum Electron.* **2016**, *22*, 4500204.
[10] E. Kifle, P. Loiko, C. Romero, J. R. V. de Aldana, V. Zakharov, A. Veniaminov, U. Griebner, V. Petrov, P. Camy, A. Braud, M. Aguiló, F. Díaz, X. Mateos, *J. Lightwave Technol.* **2020**, *38*, 4374.
[11] Y. Jia, C. Cheng, J. R. V. de Aldana, G. R. Castillo, B. del Rosal Rabes, Y. Tan, D. Jaque, F. Chen, *Sci. Rep.* **2014**, *4*, 5988.
[12] H. Liu, C. Cheng, C. Romero, J. R. V. de Aldana, F. Chen, *Opt. Express* **2015**, *23*, 9730.
[13] R. Lacovara, H. K. Choi, C. A. Wang, R. L. Aggarwal, T. Y. Fan, *Opt. Lett.* **1991**, *16*, 1089.
[14] E. Innerhofer, T. Südmeyer, F. Brunner, R. Häring, A. Aschwanden, R. Paschotta, C. Hönninger, M. Kumkar, U. Keller, *Opt. Lett.* **2003**, *28*, 367.
[15] J. Siebenmorgen, T. Calmano, K. Petermann, G. Huber, *Opt. Express* **2010**, *18*, 16035.
[16] T. Calmano, J. Siebenmorgen, A.-G. Paschke, C. Fiebig, K. Paschke, G. Erbert, K. Petermann, G. Huber, *Opt. Mater. Express* **2011**, *1*, 428.
[17] S. Y. Choi, T. Calmano, M. H. Kim, D.-I. Yeom, C. Kränkel, G. Huber, F. Rotermund, *Opt. Express* **2015**, *23*, 7999.
[18] M. H. Kim, T. Calmano, S. Y. Choi, B. J. Lee, I. H. Baek, K. J. Ahn, D.-I. Yeom, C. Kränkel, F. Rotermund, *Opt. Mater. Express* **2016**, *6*, 2468.
[19] Y. Ren, C. Cheng, Y. Jia, Y. Jiao, D. Li, M. D. Mackenzie, A. K. Kar, F. Chen, *Opt. Mater. Express* **2018**, *8*, 1633.
[20] J. E. Bae, T. G. Park, E. Kifle, X. Mateos, M. Aguiló, F. Díaz, C. Romero, J. R. V. de Aldana, H. Lee, F. Rotermund, *Opt. Lett.* **2020**, *45*, 216.
[21] J. E. Bae, S. Y. Choi, C. Kränkel, K. Hasse, F. Rotermund, *Curr. Opt. Photon.* **2021**, *5*, 180.
[22] R. Mary, G. Brown, S. J. Beecher, F. Torrisi, S. Milana, D. Popa, T. Hasan, Z. Sun, E. Lidorikis, S. Ohara, A. C. Ferrari, A. K. Kar, *Opt. Express* **2013**, *21*, 7943.
[23] S. Y. Choi, T. Calmano, F. Rotermund, C. Kränkel, *Opt. Express* **2018**, *26*, 51403.
[24] J. E. Bae, X. Mateos, M. Aguiló, F. Díaz, J. R. V. de Aldana, C. Romero, H. Lee, F. Rotermund, *Opt. Express* **2020**, *28*, 18027.
[25] Z. Li, C. Pang, R. Li, F. Chen, *J. Phys. Photonics* **2020**, *2*, 031001.
[26] P. Avouris, M. Freitag, V. Perebeinos, *Nat. Photon.* **2008**, *2*, 341.
[27] F. Bonaccorso, Z. Sun, T. Hasan, A. C. Ferrari, *Nat. Photon.* **2010**, *4*, 611.
[28] S. Hakobyan, V. J. Wittwer, K. Hasse, C. Kränkel, T. Südmeyer, T. Calmano, *Opt. Lett.* **2016**, *41*, 4715.
[29] H. R. Stuart, *Science* **2000**, *289*, 281.
[30] W. Shi, Y. Tian, A. Gervais, *Nanophotonics* **2020**, *9*, 4629.